International Journal of Heat and Fluid Flow 30 (2009) 211–217

Contents lists available at ScienceDirect

International Journal of Heat and Fluid Flow

journal homepage: www.elsevier.com/locate/ijhff

Heat transfer in rotating cylindrical cells with partitions

Thaveesak Boonpongmanee, Yasuhiro Kamotani *

Department of Mechanical and Aerospace Engineering, Case Western Reserve University, 10900 Euclid Avenue, Cleveland, OH 44106, USA

ARTICLE INFO

Article history:
Received 1 February 2008
Received in revised form 25 November 2008
Accepted 8 December 2008
Available online 20 January 2009

Keywords:
Convection heat transfer
Rotating flow
Ekman layer
Partitions

ABSTRACT

A numerical analysis and an experimental study of heat transfer rate in rotating cylindrical cells with partitions are performed. The work is done mainly in the Ekman suction regime, where the Coriolis force dominates over centrifugal buoyancy. It is shown that the heat transfer rate increases substantially by placing partitions in the cell. The partitions suppress the Coriolis force so that convection induced by the centrifugal buoyancy becomes important. It is found that the Nusselt number correlates with the parameter $Pr\beta\Delta TEk^{-1/2}$ with the partitions. The partitions have no effect on the heat transfer in the centrifugal buoyancy convection regime.

1. Introduction

Advanced life support systems and waste treatment systems will become increasingly important in future long-duration space missions (Committee on Microgravity Research, 2000). A significant problem in the development of life support systems in microgravity is insufficient knowledge concerning fluid motion. One effective way to induce fluid flow in the presence of density gradients (for increased heat or mass transfer) is to use rotation (centrifugal acceleration). Also, the performance of rotating electrochemical cells in microgravity has been extensively investigated by our group (e.g. Weng et al., 1998). Flows in rotating systems with heat or mass transfer are also of scientific interest because of complex interactions among centrifugal and gravitational buoyancy, Coriolis and viscous forces. Heat transfer in rotating cylindrical cells with their axes aligned with gravity has been studied by several investigators in the past, theoretically (Barcilon and Pedlosky, 1967; Homsy and Hudson, 1969), experimentally (Hudson et al., 1978), numerically (Chew, 1985; Guo and Zhang, 1992; Brummell et al., 2000), among many others. Those studies were performed under negligible gravity or the heat-from-above configuration. Mass transfer in rotating shallow electrochemical cells was investigated experimentally (Weng et al., 1998) and numerically (Weng et al., 2000). Weng et al. (1998) also performed a scaling analysis of heat and mass transfer in rotating cells to determine the flow and boundary layer characteristics. They delineated two convection mechanisms for the boundary layer regime: one is centrifugal buoyancy dominated convection and the other is called Ekman suction convection. In the Ekman suction regime, the Coriolis force suppresses centrifugal buoyancy, inhibiting the heat transfer rate. In some applications it is desirable to increase the heat or mass transfer rate (e.g. electrochemical applications in microgravity). Since the Coriolis force is associated with the azimuthal flow, the heat transfer rate can be increased by placing partitions in the cell in order to suppress the azimuthal flow and thus the Coriolis force. For this reason the effect of partitions on the flow and heat transfer in rotating cylindrical cells is investigated mainly numerically in this work. Experimental work is also performed to validate some of the numerical results. The work is done mainly under the condition that gravitational buoyancy is negligible.

2. Mathematical formulation and important dimensionless parameters

The flow and heat transfer in rotating cells are investigated mainly numerically in this work. Fig. 1 is a schematic of rotating cylinder with partitions. The (r,θ,z) coordinate system, defined in Fig. 1, is attached to the rotating container. The flow is assumed to be steady and laminar. The modified Boussinesq approximation is employed, namely the fluid density is variable only in the centrifugal and gravitational terms, which gives rise to centrifugal buoyancy and gravitational buoyancy, respectively. The coordinates r and z are non-dimensionalized by R and H, respectively. The velocities (u,v,w) are made dimensionless by $R\Omega\beta\Delta T$, $R\Omega\beta\Delta T$, and $R\Omega\beta\Delta T$ Ar, respectively, based on the scaling analysis by Weng et al. (1998). The pressure p is modified from the original pressure p^* as $p = p^* + \rho gz - \rho\Omega^2 r^2/2$. The modified pressure p is non-dimen-

* Corresponding author. Tel.: +1 216 368 6455.
E-mail addresses: txb42@case.edu (T. Boonpongmanee), yxk@case.edu (Y. Kamotani).

0142-727X/$ - see front matter © 2008 Elsevier Inc. All rights reserved.
doi:10.1016/j.ijheatfluidflow.2008.12.002

Nomenclature

Symbols

Ac	ratio of gravitational to centrifugal acceleration, $g/\Omega^2 R$
Ar	aspect ratio, H/R
Ek	Ekman number, $\nu/\Omega H^2$
g	gravitational acceleration (m/s^2)
h	heat transfer coefficient ($W/m^2\,°C$)
H	height of test cell (m)
K	thermal conductivity (W/m °C)
NP	number of partitions
Nu	Nusselt number, hH/k
P	modified pressure, $p = p^* + \rho g z - \rho\Omega^2 \mathbf{r}^2/2$ (Pa)
p^*	pressure (Pa)
Pr	Prandtl number, ν/α
r	radial coordinate (m)
R	radius of test cell (m)
Ro_T	thermal Rossby number, $\beta\Delta T$
T	temperature (°C)
T_C	cold wall temperature (°C)
T_H	hot wall temperature (°C)
(u,v,w)	velocity components (m/s)
U	radial reference velocity (m/s)
Z	axial coordinate (m)

Greek symbols

α	thermal diffusivity (m^2/s)
β	volumetric expansion coefficient (1/°C)
δ_T	thermal boundary layer thickness (m)
δ_V	velocity boundary layer thickness (m)
ΔT	temperature difference, $T_H - T_C$ (°C)
θ	azimuthal angle (rad)
θ_0	sector opening angle (rad)
ν	kinematic viscosity (m^2/s)
Ω	rotation rate (rad/s)
ρ	density (kg/m^3)

sionalized by $\mu\Omega\beta\Delta T$. The temperature is non-dimensionalized as $(T - T_C)/\Delta T$. The following dimensionless equations are solved.

Continuity equation:

$$\frac{\partial}{\partial r}(ru) + \frac{\partial}{\partial \theta}(rv) + \frac{\partial}{\partial z}(rw) = 0 \tag{1}$$

Momentum equations:

$$\beta\Delta T\left(u\frac{\partial u}{\partial r} + \frac{1}{r}v\frac{\partial u}{\partial \theta} + w\frac{\partial u}{\partial z} - \frac{v^2}{r}\right) = 2v - rT - Ar^2 Ek\frac{\partial p}{\partial r} + Ek\left(\nabla^2 u - \frac{u}{r^2} - \frac{2}{r^2}\frac{\partial v}{\partial \theta}\right) \tag{2}$$

$$\beta\Delta T\left(u\frac{\partial v}{\partial r} + \frac{1}{r}v\frac{\partial v}{\partial \theta} + w\frac{\partial v}{\partial z} + \frac{uv}{r}\right) = -2u + Ek\left(\nabla^2 v - \frac{v}{r^2} + \frac{2}{r^2}\frac{\partial u}{\partial \theta}\right) \tag{3}$$

$$\beta\Delta T\left(u\frac{\partial w}{\partial r} + \frac{1}{r}v\frac{\partial w}{\partial \theta} + w\frac{\partial w}{\partial z}\right) = \frac{Ac}{Ar}T - Ek\frac{\partial p}{\partial z} + Ek\nabla^2 w \tag{4}$$

where $\nabla^2 = \frac{1}{r}\frac{\partial}{\partial r}\left(r\frac{\partial}{\partial r}\right) + \frac{1}{r^2}\frac{\partial^2}{\partial \theta^2} + \frac{\partial^2}{\partial z^2}$.

Energy equation:

$$\beta\Delta T\left(u\frac{\partial T}{\partial r} + \frac{1}{r}v\frac{\partial T}{\partial \theta} + w\frac{\partial T}{\partial z}\right) = \frac{Ek}{\mathrm{Pr}}\nabla^2 T \tag{5}$$

As for the boundary conditions, all the velocities vanish on the walls (top, bottom, outer and partition walls). The top and bottom walls are maintained at uniform temperatures (T_H or T_C). The outer and partition walls are thermally insulated. The partitions are equally spaced in the azimuthal direction.

Several important parameters appear in the above equations: Ek (Ekman number) = $\nu/\Omega H^2$, Ro_T (thermal Rossby number) = $\beta\Delta T$, Pr (Prandtl number) = ν/α, Ar (container aspect ratio) = H/R, and Ac (gravitational to centrifugal acceleration ratio) = $g/\Omega^2 R$. From the above equations one sees that Ek represents the ratio of viscous to Coriolis forces, and $\beta\Delta T$ represents the ratio of inertia to Coriolis forces. The ratio of gravitational to centrifugal buoyancy forces scales as Ac/Ar. The overall heat transfer coefficient (h) is computed from the total heat transfer rate through the liquid and the imposed temperature difference, which is then non-dimensionalized as the average Nusselt number (Nu = hH/k).

This work covers the following parametric ranges: $0.7 \leqslant \mathrm{Pr} \leqslant 3000$ (mainly Pr = 7), $0.002 \leqslant \beta\Delta T \leqslant 0.2$, $0.3 \leqslant \mathrm{Ar} \leqslant 1.4$, and $2 \times 10^{-5} \leqslant \mathrm{Ek} \leqslant 10^{-2}$. Ac = 0, except when the numerical results are compared with experimental data. This work is directly applicable to the corresponding mass transfer problem if we replace ΔT by ΔC (C, concentration), Pr by Schmidt number, and Nu by Sherwood number (Weng et al., 1998). The above range of Pr is selected because the Schmidt number can be as large as 3000 in electrochemical applications (Weng et al., 1998).

The flow structure is well known for axisymmetric flow in rotating cylinders. According to the scaling analysis by Weng et al. (1998), the flow structure is fundamentally different depending on the range of combined parameter $\mathrm{PrRo_T} = \mathrm{Pr}\beta\Delta T$. When the

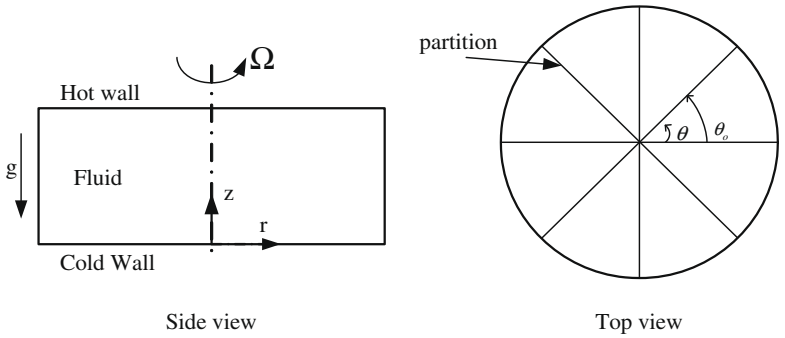

Fig. 1. Schematic of rotating cylinder with partitions.

parameter is less than unity, the flow structure is in the so-called Ekman suction regime, in which the thermal boundary layer is thicker than the Ekman layer. The thickness of the Ekman layer (δ_V) is proportional to $\delta_V \sim (\nu/\Omega)^{1/2}$. The radial velocity (u-velocity) is confined to this Ekman layer. The radial flow is outward along the cold wall and inward along the hot wall. The radial flow gives rise to azimuthal flow through the Coriolis force (the first term on the right-hand side of Eq. (3)). The azimuthal flow direction is such that it is slower than the solid-body rotation speed in the region where the radial velocity is outward (or faster when the radial velocity is inward). The azimuthal flow in return affects the radial flow through the Coriolis force in the radial direction (the first term on the right-hand side of Eq. (2)). The radial flow is much suppressed in the core region, the region outside the Ekman layers, by this interaction. In the present work the main quantity of interest is the heat transfer rate between the hot and cold walls or the Nusselt number. According to the scaling law obtained in Weng et al. (1998), Nu scales with the combined parameter $Pr\beta\Delta TEk^{-1/2}$. If partitions are placed in the cell, they obstruct the strong azimuthal flow, which alters the flow structure substantially. Therefore, the Ekman suction regime is of the main interest in this work.

3. Numerical modeling

Without partitions the flow is axisymmetric (or two-dimensional) and we have investigated the flow numerically in our past work (Weng et al., 2000). It was based on the SIMPLEC algorithm (Doormael and Raithby, 1984), and the scheme employed is explained in detail in Weng et al. (2000). We use the same program in the present axisymmetric flow analysis. A non-uniform grid system is employed with meshes graded towards the walls. For the conditions of $Ek = 5 \times 10^{-5}$, $\beta\Delta T = 0.01$, Ar = 0.5, and Ac = 0, the values of Nu computed with three different grids, 40×46 ($r \times z$), 60×67, and 80×90 with the smallest axial mesh sizes next to the top and bottom walls of 0.003, 0.001, and 0.0005 are 1.88, 1.85, 1.85, respectively. Therefore, the 60×67 grid system is used.

The above scheme is extended to three dimensions to analyze the flow with partitions. It is found that the same 60×67 grid system used in the axisymmetric flow analysis is also good in the 3D analysis. A non-uniform grid system is used in the azimuthal direction. For the same conditions as above but with two partitions, the values of Nu computed with three different numbers of azimuthal grids, 25, 37, and 58 with the smallest mesh sizes next to the partitions of 0.005, 0.003, and 0.002, respectively, are 5.33, 5.40, and 5.41. Therefore, the $60 \times 67 \times 37$ ($r \times z \times \theta$) grid system is used in the present analysis. The computations are done on a three-node 64-bit LINUX commodity cluster.

4. Experimental work

Some results of the numerical analysis are validated by experimental data. The experimental apparatus is the same as the one used in our past experiment (Weng et al., 1998; Boonpongmanee, 2005), so it is not described in detail herein. In this work, the top wall is heated and the bottom wall is cooled. The test fluid is water. A motor with a gear reducer is used to rotate a frame which holds the test cell. The bottom wall of the test cell is made of 0.64 cm thick copper plate and is one wall of a cooling chamber. A rotating fluid joint is used to transport water to the cooling chamber. The top wall is also made of 0.64 cm thick copper plate with a heating mat attached to one side. The other side of the heating mat is insulated by 2.5 cm thick fiberglass. The sidewall is made of lexan tube with 1.27 cm thickness. The outer surface of the sidewall is insulated by fiberglass. The inner diameter of the test section is 15.0 cm and its height is set at 5.0 cm (Ar = 0.67) and 3.5 cm (Ar = 0.47). Thermocouples are imbedded in the top and bottom walls, three in each wall, to monitor the temperatures. Those thermocouples are positioned randomly in the radial and azimuthal directions. Since they do no show systematic temperature variations in any test within the experimental error, three thermocouples are judged to be sufficient. A slip ring is mounted at the bottom frame to transfer the signals and supply electricity to the cell. The partitions are made of 3.2 mm thick plexiglass.

After the power to the heater is started, we usually wait 3–4 h for a thermal equilibrium. The heat transfer in this situation is predominantly by conduction. Because of some technical difficulties, the rotating system cannot be rotated continuously that long. Therefore, we start to rotate the cell after the thermal equilibrium. The temperature field is found to become steady within about 1 h of the start of rotation. The rotation speed is kept within 1% accuracy within this time. The top and bottom wall temperatures are recorded continuously, from which the overall heat transfer coefficient (h) is determined as a function of time. A system manufactured by Gould (Model 7700 series) is used for data acquisition. Although the cell is carefully insulated, not all the heater power input is given to the liquid. Some heat is lost from the other side of heater and some is given to the clod wall through the sidewall. From various tests without rotation, we estimate the heat loss to be about 20–30%, mostly depending on ΔT, under the present experimental conditions. We use the net heat input to the liquid to determine h, which is then non-dimensionalized as the average Nusselt number ($Nu = hH/k$). The total experimental error in Nu is estimated to be ±10%.

5. Results and discussion

5.1. Comparison with experimental data

The numerically predicted Nu is compared with the experimental data in Fig. 2 with and without partitions. Nu is computed with gravity. Since the top wall is heated in the experiment, gravitational buoyancy opposes the main flow, so Nu decreases with gravity. Ac ranges from 0.6 to 2.4 in the experiment. As seen in Fig. 2, the numerical and experimental results agree well within the experimental error. Fig. 2 shows that the partitions increase the heat transfer rate substantially. It is found that when the rotation speed becomes high (greater than about 300 rpm), the convective cooling of the test cell by the surrounding air becomes important

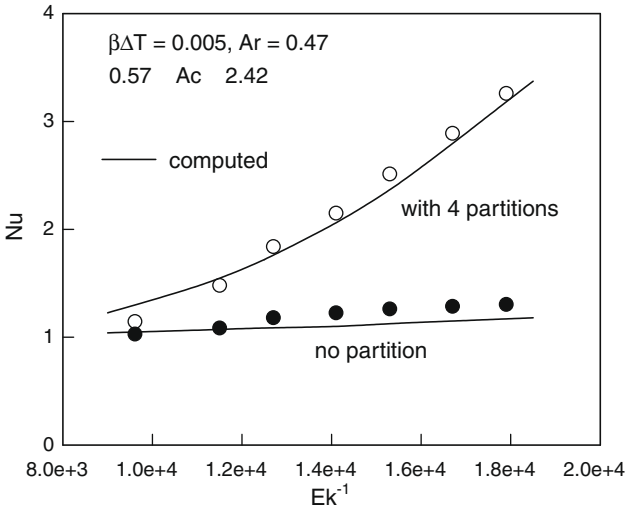

Fig. 2. Comparison of experimental and numerical Nu.

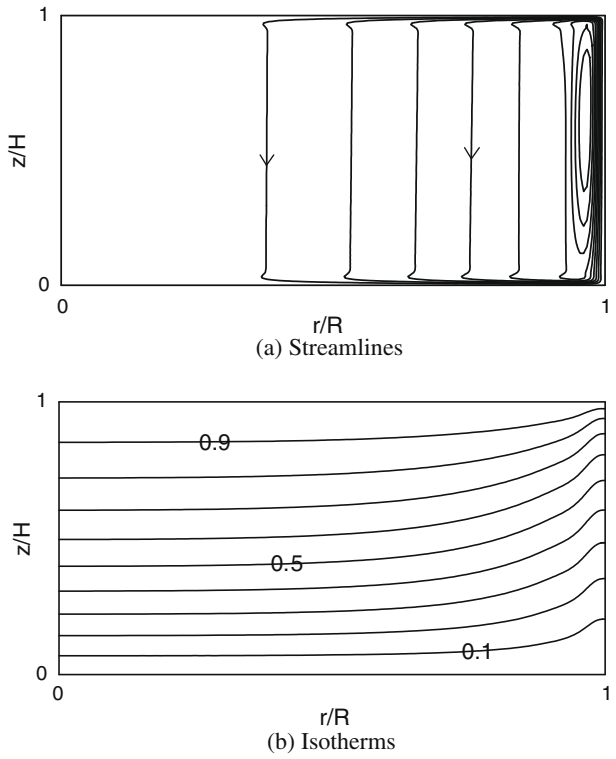

Fig. 3. Streamlines and isotherms (Ek = 10^{-4}, $\beta\Delta T = 0.005$, Ac = 0, Ar = 0.5, Pr = 7, NP = 0).

and the heat loss increases. For this reason we do not go beyond around 300 rpm in the present experiment.

5.2. Flow and temperature fields without partitions

The velocity and temperature fields are shown for one typical case in Fig. 3. They show streamlines and isotherms in a meridional plane. The meridional streamlines are constructed from the u and w velocities. In the figure, the streamlines are equally spaced from the maximum value to the wall. The flow structure is counterclockwise unicellular. Thin velocity boundary layers can be recognized along the horizontal walls. The upward flow is confined to a small region next the outer wall. The downward flow, which exists over most of the meridional plane, is called the Ekman suction. The suction flow is due to the entrainment and detrainment by the bottom and top boundary layers, respectively. The suction flow is nearly vertically downward, which means that the radial velocity is very small in the core region.

The isotherms of Fig. 3 show that the temperature field is almost vertically stratified. The confined upward flow along the outer wall causes a thin thermal boundary layer near the outer edge of the top wall, where large heat transfer takes place. Outside this region over the top wall, the Ekman suction thickens the thermal boundary layer. In contrast, the suction flow thins the thermal boundary layer over the bottom wall, and heat transfer is more uniform.

One important feature of flow in the Ekman suction regime is that the radial flow is suppressed by the Coriolis force associated with the azimuthal flow. The velocity distributions at $r/R = 0.5$ are shown in Fig. 4 for the conditions of Fig. 3. As seen in the figure, the radial flow occurs only in the very thin Ekman layers. As discussed in Weng et al. (2000), the Coriolis force is balanced by the centrifugal buoyancy in the core region. The centrifugal buoyancy, which is related to the temperature variation in the vertical direction, exists rather uniformly everywhere in the container, so the azimuthal flow exists everywhere and suppresses the radial flow in the core. Consequently, although the main driving force of the flow exists in the radial direction, the azimuthal velocity is much larger than the radial velocity.

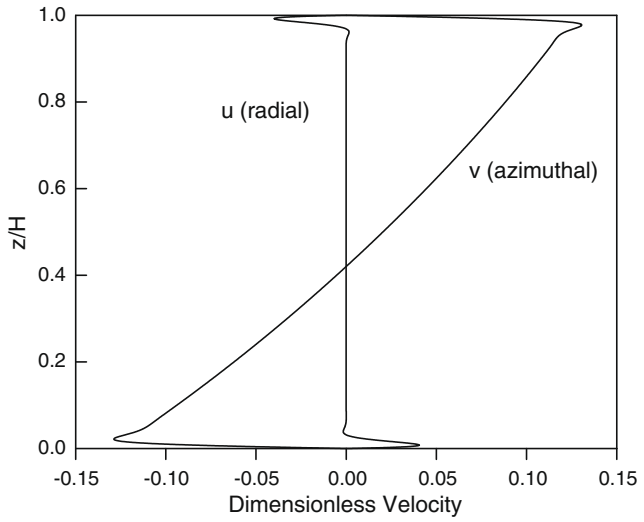

Fig. 4. Velocity distributions at $r/R = 0.5$ (Ek = 10^{-4}, $\beta\Delta T = 0.005$, Ac = 0, Ar = 0.5, Pr = 7, NP = 0).

As mentioned earlier, Nu scales with combined parameter $Pr\beta\Delta TEk^{-1/2}$ in the Ekman suction regime. In order to prove the scaling law, values of Nu are computed under various conditions and presented in Fig. 5. The experimental data are also shown. Since the computations are done for Ac = 0, the experimental data for Ac < 1 are shown. As Fig. 5 shows, Nu computed under various conditions can be correlated by the combined parameter. The Ekman suction regime is fully-established, namely Nu becomes proportional to $Pr\beta\Delta TEk^{-1/2}$, when the parameter is larger than about 10. The experimental data tend to be smaller than the computed values due to gravity but roughly follow the numerical values.

Although the axial velocity is relatively large, there is no temperature gradient in the azimuthal direction, so it does not contribute directly to the heat transfer. Therefore, if one can utilize this

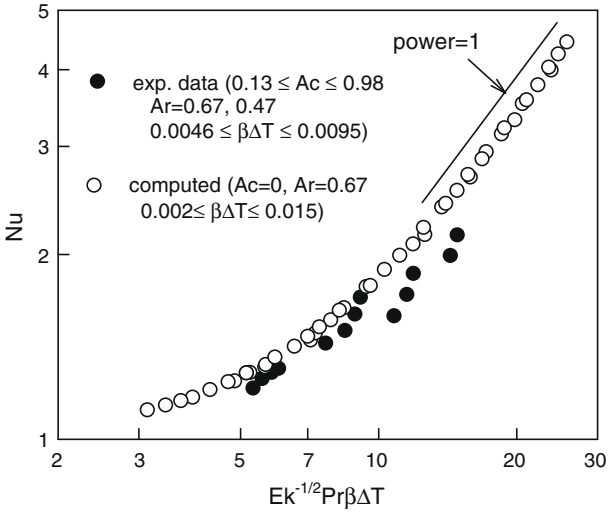

Fig. 5. Scaling law for Nu in Ekman suction regime.

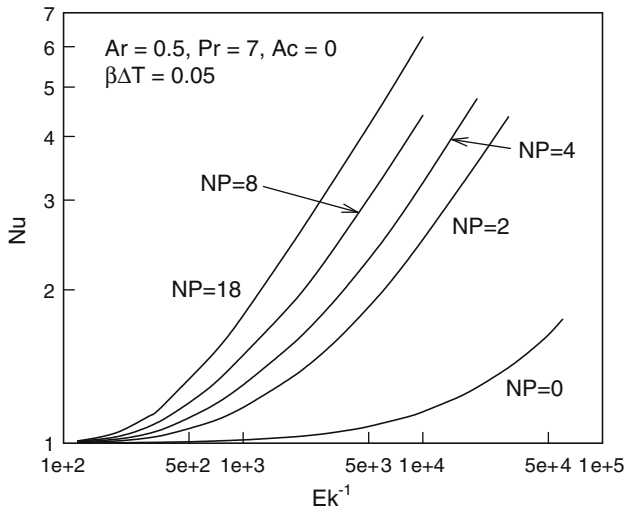

Fig. 6. Effect of number of partitions on Nu.

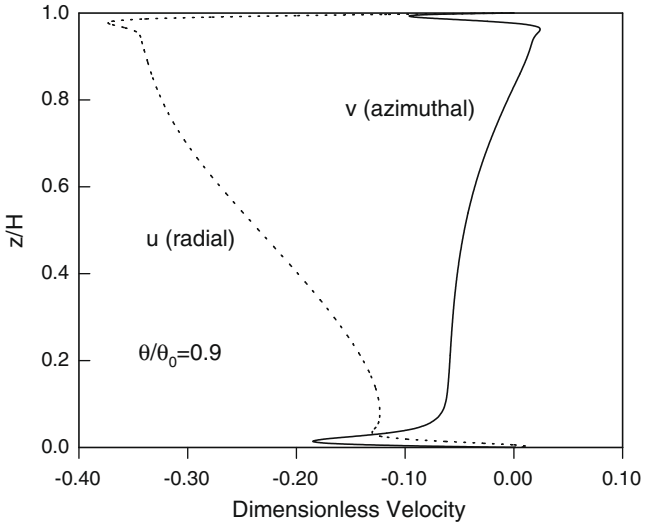

(a) Velocity distributions at $\theta/\theta_0 = 0.9$.

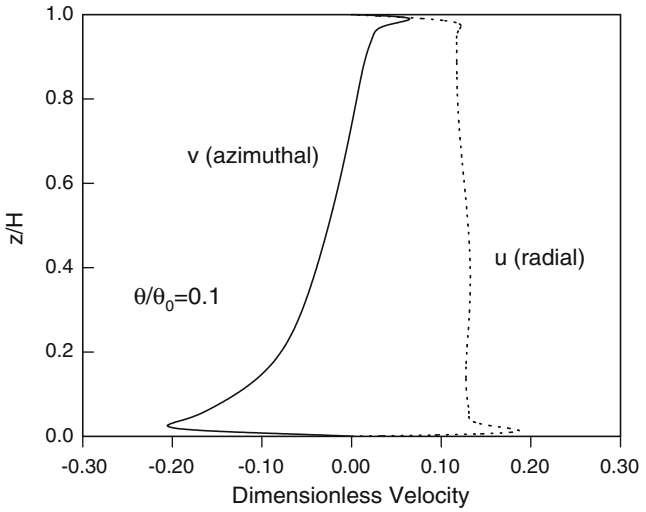

(b) Velocity distributions at $\theta/\theta_0 = 0.1$.

Fig. 7. Velocity distributions at $r/R = 0.5$ with partitions (Ek = 10^{-4}, $\beta\Delta T = 0.005$, Ac = 0, Ar = 0.5, Pr = 7, NP = 8).

azimuthal flow for mixing the hot and cold fluid, the heat transfer rate will increase. This is the basic idea behind the usage of partitions.

5.3. Flow and temperature fields with partitions

5.3.1. Basic picture

Fig. 6 shows how the partitions affect Nu when Ek and NP are varied. When Ek is sufficiently large, the heat transfer is dominated by conduction (Nu = 1), so the partitions have no effect on Nu. As Ek decreases, convection becomes increasingly important and the heat transfer rate is increasingly augmented by the partitions. Even with only two partitions, the increase is significant when Ek is small. The effect of NP becomes increasingly significant with decreasing Ek. It is found that, for a given Ek, Nu increases monotonically with increasing NP when NP is varied from 2 to 18. For example, Nu increases from 2.51 for NP = 2–6.27 for NP = 18 at Ek = 10^{-4}. In reality, the partition wall has a finite thickness, so NP greater than 20 may not be practical. The fact that the partitions can increase the heat transfer rate several times has important practical implications.

The main effect of the partitions on the flow is as follows. As discussed earlier, the Coriolis force in the radial direction is balanced by centrifugal buoyancy in the core region in axisymmetric flow. As a result, the core region is dominated by counter-flowing azimuthal flow (Fig. 4). The partitions force this azimuthal flow to recirculate within the sector. When the azimuthal flow along the

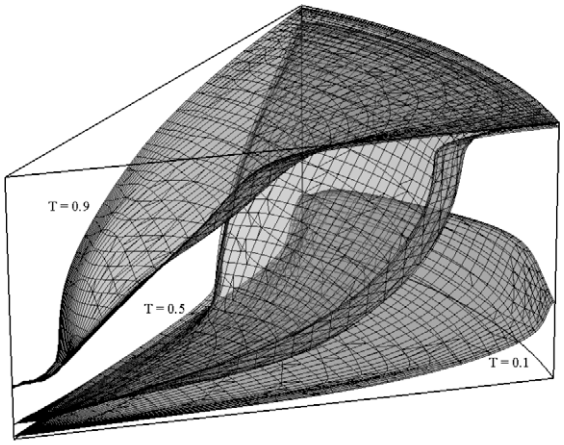

(a) Isotherm planes

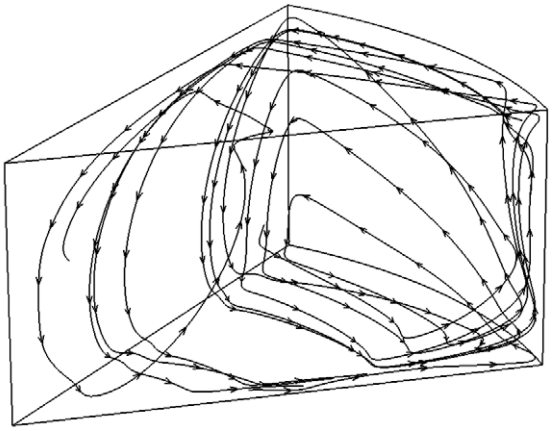

(b) Streamlines

Fig. 8. Isotherm planes and streamlines with partitions (Ek = 10^{-4}, $\beta\Delta T = 0.005$, Ac = 0, Ar = 0.5, Pr = 7, NP = 8).

top (hot) wall, which is moving towards the wall at $\theta = \theta_0$, hits the partition, the azimuthal velocity and thus the Coriolis force in the radial direction is reduced. As a result, the buoyancy force dominates, which causes radially inward flow along the partition at $\theta = \theta_0$. Typical velocity distributions are shown in Fig. 7 and 7a shows strong radially inward flow across the depth of the container at $\theta/\theta_0 = 0.9$. Similarly, when the azimuthal flow along the bottom wall hits the partition at $\theta = 0$, the buoyancy force causes radially outward flow along the partition wall (see Fig. 7b). In order to show the overall flow structure, some streamlines mainly near the walls are shown in Fig. 8. One can see a general recirculating pattern caused by the azimuthal flow. The radial flow along the partition at $\theta = 0$ results in a strong upward flow at the corner of the partition and the outer wall. In contrast, the downward flow is more spread over the partition at $\theta = \theta_0$. The three-dimensional isotherm pattern presented in Fig. 8 shows that they are very much distorted compared to those without the partitions shown in Fig. 3, indicating an increased heat transfer rate.

5.3.2. Effects of various parameters

Without the partitions Nu scales with the combined parameter $Pr\beta\Delta TEk^{-1/2}$ in the Ekman suction regime (Fig. 5). Since the Ekman suction dominates, this parameter is obtained by balancing the axial convection (Ekman suction) and the conduction in the thermal boundary layer (Weng et al., 1998). With the partitions, it is found that Nu does not correlate with $Pr\beta\Delta TEk^{-1/2}$. This suggests that the heat transfer mechanism is changed with the partitions. It is found that Nu can be correlated by the parameter $(Pr\beta\Delta T)^{1/2}Ek^{-1/2}$ for a fixed NP (Fig. 9). Nu becomes proportional to the parameter when the parameter is above about 15 for NP = 2 and above 10 for NP = 8. This scaling law can be explained as follows. As discussed above, the radial convection becomes important with the partitions. Then, by balancing the radial convection and the conduction in the thermal boundary layer one obtains the scaling law $\delta_T/H \sim (\alpha/UHAr)^{1/2}$, where U is the characteristic radial velocity. Nu scales with H/δ_T. Since the radial velocity is induced by the centrifugal buoyancy, it scales with $\beta\Delta TR\Omega$, from which it can be shown that $Nu \sim (Pr\beta\Delta T)^{1/2}Ek^{-1/2}$. Therefore, the correlation in Fig. 9 is consistent with the aforementioned flow structure change caused by the partitions.

Fig. 10 shows the effect of Ar on Nu. Although Nu decreases monotonically with increasing Ar for a given Ek, its effect is not significant in the ranges of Ar and Ek investigated. Increasing Ar for a given Ek means in practice to increase R while keeping the fluid, rotation rate and H the same. Since the centrifugal buoyancy increases with increasing radius, the driving force is effectively used in shallow enclosures (small Ar) but increased viscous effects of the walls counter-balance this, resulting in a relatively weak effect of Ar.

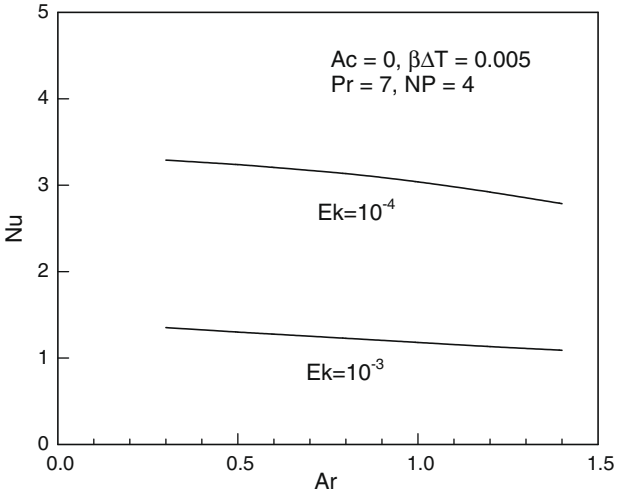

Fig. 10. Effect of Ar on Nu with partitions.

When the parameter $Pr\beta\Delta T$ becomes larger than unity, we get into the centrifugal buoyancy convection regime, where the thermal boundary layer is thinner than the Ekman layer and the centrifugal buoyancy dominates over the Coriolis forces. Generally this happens when Pr is large. Also, in the case of corresponding mass transfer problem, this regime results when the Schmidt number is large. According to the scaling analysis by Weng et al. (1998), Nu scales with $Ek^{-1/2}(Pr\beta\Delta T)^{1/4}$ in this regime. Since the Coriolis forces are not dominant, the partitions are not expected to have strong effect on the heat transfer. To show this, Nu is computed in the range $Pr\beta\Delta T \geqslant 1$ in Fig. 11. In order to be consistent with the Nu scaling laws for the two regimes, $NuEk^{1/2}$ is plotted against $Pr\beta\Delta T$ in Fig. 11. The figure shows that the values of $NuEk^{1/2}$ computed under various conditions can be correlated by the parameter PrβΔT, including the intermediate regime where $Pr\beta\Delta T \sim 1$. The centrifugal buoyancy convection regime is fully established, namely $NuEk^{1/2} \sim (Pr\beta\Delta T)^{1/4}$, when $Pr\beta\Delta T$ is larger than about 100. With the partitions, Nu is slightly increased when PrβΔT is

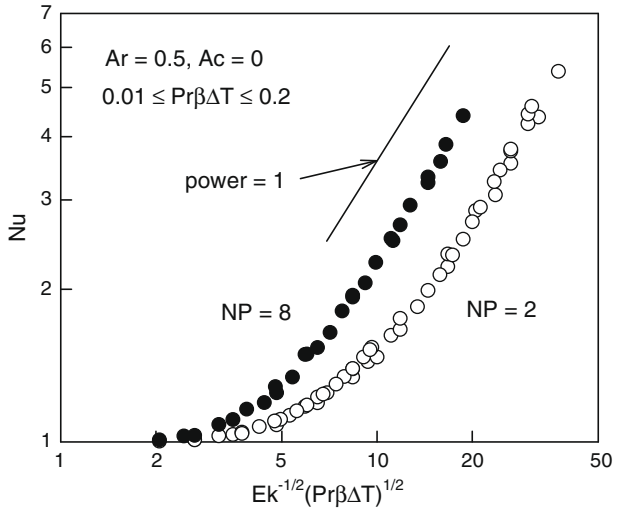

Fig. 9. Correlation of computed Nu with partitions.

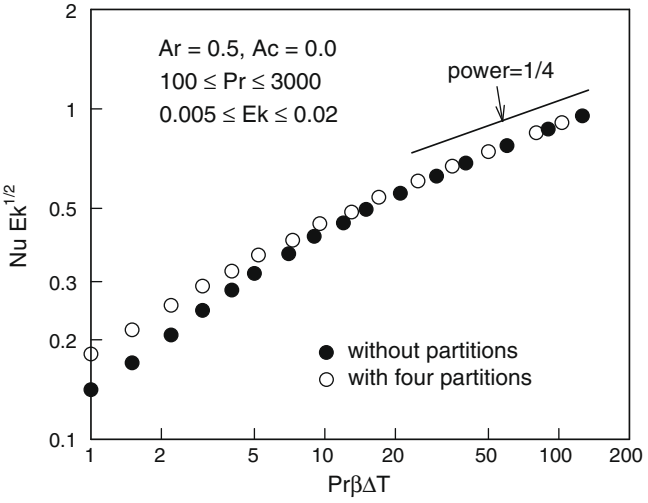

Fig. 11. Effect of partitions on Nu in centrifugal buoyancy convection regime.

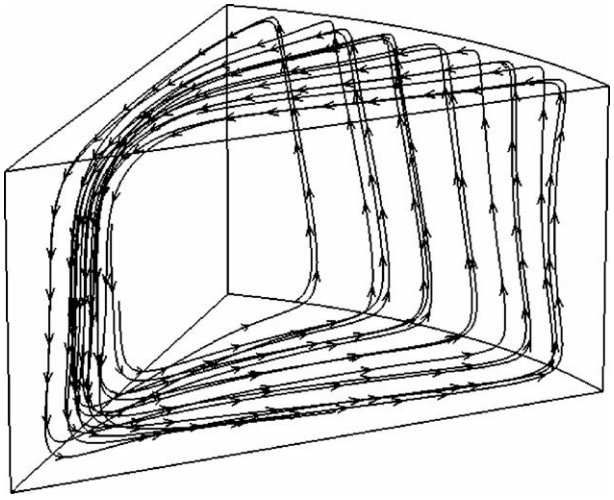

Fig. 12. Streamlines with partitions in centrifugal buoyancy convection regime ($Ek = 10^{-2}$, $\beta\Delta T = 0.02$, $Pr\beta\Delta T = 30$, Ac = 0, Ar = 0.5, NP = 8).

less than 10, but they have no effect on Nu when the regime is fully established. The streamlines are shown in Fig. 12 for this regime. Compared to Fig. 8b, it is clear that the flow is mainly in the radial direction so that the partitions have no appreciable effect.

6. Conclusions

Heat transfer in rotating cylindrical cells with partitions is investigated mainly numerically. The numerical scheme is validated against the experimental data obtained in this work. The results show that the heat transfer rate increases substantially by placing partitions in the cell in the Ekman suction regime. The radial flow, which is suppressed by the Coriolis force without the partitions, becomes active as the azimuthal flow slows near the partitions. The Nusselt number (Nu) increases monotonically with increasing number of partitions (NP) up to NP = 18 (the largest NP investigated herein). It is shown that Nu correlates with the parameter $Pr\beta\Delta TEk^{-1/2}$ for a given NP. The partitions create a complex three-dimensional flow structure. In contrast, the partitions have no effect on the heat transfer in the centrifugal buoyancy convection regime, since the Coriolis force is not important in this regime. The flow structure remains nearly axisymmetric with the partitions.

Acknowledgment

This work was supported by NASA Cooperative Agreement NCC3-823.

References

Barcilon, V., Pedlosky, J., 1967. On the steady motions produced by a stable stratification in a rapidly rotating fluid. Journal of Fluid Mechanics 29 (3), 673–690.

Boonpongmanee, T., 2005. Numerical and experimental investigation of heat and mass transfer in rotating systems. Ph. D. thesis, Case Western Reserve University, Cleveland, Ohio.

Brummell, N., Hart, J.E., Lopez, J.M., 2000. On the flow induced by centrifugal buoyancy in a differentially-heated rotating cylinder. Theoretical and Computational Fluid Dynamics 14, 39–54.

Chew, J.W., 1985. Computation of convective laminar flow in rotating cavities. Journal of Fluid Mechanics 153, 339–360.

Committee on Microgravity Research, National Research Council, 2000. Microgravity Research in Support of Technologies for the Human Exploration and Development of Space and Planetary Bodies. National Academy Press, Washington, DC.

Doormael, J.P., Raithby, G.D., 1984. Enhancement of the SIMPLE method for predicting incompressible fluid flows. Numerical Heat Transfer 7, 147–163.

Guo, Z.-Y., Zhang, C.-M., 1992. Thermal drive in centrifugal fields-mixed convection in a vertical rotating cylinder. International Journal of Heat Mass Transfer 35, 1635–1644.

Homsy, G.M., Hudson, J.L., 1969. Centrifugally driven thermal convection in a rotating cylinder. Journal of Fluid Mechanics 35 (1), 33–52.

Hudson, J.L., Tang, D., Abell, S., 1978. Experiments on centrifugally driven thermal convection in a rotating cylinder. Journal of Fluid Mechanics 86 (1), 147–159.

Weng, F.B., Kamotani, Y., Ostrach, S., 1998. Mass transfer rate study in rotating shallow electrochemical cells. International Journal of Heat Mass Transfer 41, 2725–2733.

Weng, F.B., Kamotani, Y., Ostrach, S., 2000. Numerical analysis of solutal convection in rotating shallow electrochemical cells. International Journal of Heat Mass transfer 43, 341–351.